

# Hallucinating Robots: Inferring Obstacle Distances from Partial Laser Measurements

Jens Lundell\*, Francesco Verdoja\* and Ville Kyrki

**Abstract**—Many mobile robots rely on 2D laser scanners for localization, mapping, and navigation. However, those sensors are unable to correctly provide distance to obstacles such as glass panels and tables whose actual occupancy is invisible at the height the sensor is measuring. In this work, instead of estimating the distance to obstacles from richer sensor readings such as 3D lasers or RGBD sensors, we present a method to estimate the distance directly from raw 2D laser data. To learn a mapping from raw 2D laser distances to obstacle distances we frame the problem as a learning task and train a neural network formed as an autoencoder. A novel configuration of network hyperparameters is proposed for the task at hand and is quantitatively validated on a test set. Finally, we qualitatively demonstrate in real time on a Care-O-bot 4 that the trained network can successfully infer obstacle distances from partial 2D laser readings.

## I. INTRODUCTION

2D laser scanners are the de facto sensors used by mobile robots for navigation, mapping, and localization as they provide distance measurements in large angular fields at fast rates thanks to their small data dimensionality [1]. However, the amount of knowledge that can be extracted from a 2D laser scan may be insufficient for some tasks like object detection and obstacle avoidance. In particular, laser sensors cannot detect glass or infer the true occupancy of complex objects such as tables. An example of this problem is presented in Fig. 1: here a robot relying only on raw 2D laser data of the scene (*i.e.*, the green dots in the figure) would see the legs of the table but not the tabletop itself, allowing it to plan and execute a trajectory through the table causing a collision and harming the robot. We refer to the distance along a certain direction to the closest point of an obstacle that the robot could collide with as the robot-to-obstacle distance.

Classical approaches overcome such limitations by utilizing richer sensor readings from, for example, RGBD cameras [2] or 3D laser scanners [3], or by fusing data between different sensors [1]. These approaches often suffer from a limited field of view and higher computational requirements of the sensors they employ. Instead, we propose a method for inferring the robot-to-obstacle distance directly from 2D laser data. This is accomplished by framing the problem as a learning task where the input is raw 2D laser distance and the output is the correct 2D robot-to-obstacle distance. In essence, the network *hallucinates* the corresponding range

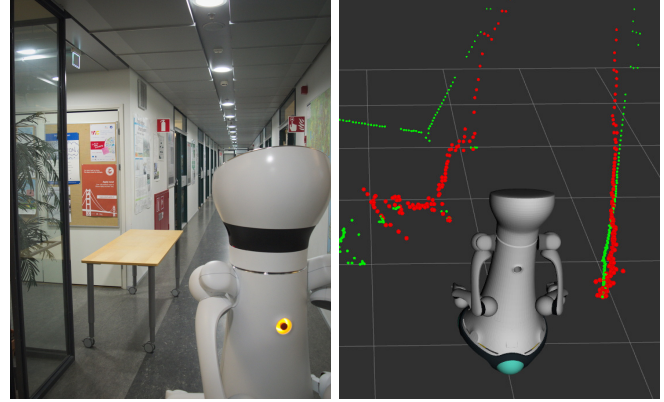


Fig. 1. A robot reconstructing the shape of a table by seeing only its legs. In the illustration on the right, the green laser is the original input signal, while the red one is the output produced in real-time by the proposed algorithm (best viewed in color).

data as if the 2D laser scanner could detect the full shape of the obstacles; hence the name *Hallucinating robots*<sup>1</sup>.

The main contributions of this work are:

- a novel approach to estimate the robot-to-obstacle distance from raw 2D laser data by training an autoencoder;
- a quantitative study over the impact on the network performance of different hyperparameters, specifically skip connections (Sect. III-B), a novel activation function tailored for the domain at hand (Sect. III-C) and data augmentation with random Gaussian noise (Sect. IV-C);
- a method to generate ground truth robot-to-obstacle distances by fusing raw 2D laser scans with overlapping depth images (Sect. IV-B);
- a qualitative evaluation of the proposed technique performed online on the real robot (Sect. IV-E) showing the method working in complex environments such as the one presented in Fig. 1 and in 360° around the robot.

To the best of our knowledge, the work presented here is the first one focusing on learning distance to otherwise invisible obstacles in 2D laser data. The hallucinated laser data is not to replace raw laser data, but instead acts as an additional source of information to enrich environment awareness and increase robot safety.

\*These authors contributed equally to this paper.

This work was supported by Academy of Finland, decision 314180.

J. Lundell, F. Verdoja and V. Kyrki are with School of Electrical Engineering, Aalto University, Finland. name.surname@aalto.fi

<sup>1</sup>Code of the implementation of the proposed method, the dataset used in this study, and a video demonstrating the algorithm running in real time on a robot can be found on our website: <http://irobotics.aalto.fi/software-and-data/hallucinating-robots>

## II. RELATED WORKS

One of the earliest works on training neural networks on laser data dates back to 1998 [4], where the trained network was used in a museum tour-guide robot to modify the initial map with the true occupancy of invisible objects such as chairs and glass showcases. That work’s scope was however limited to the exact setting where it was proposed. Only recently, mostly due to the growing possibilities of deep learning, a lot of new work has been proposed using neural networks trained on laser data [5]–[10].

In the context of obstacle detection, the use of neural networks has been proposed to infer bounding boxes of pedestrians and vehicles from 3D laser data of typical road scenes [6], [8] and to track spatially occluded moving objects in the scene by incorporating consecutive laser measurements to include the temporal information [7]. These works, however, are not directly dealing with the problem of inferring robot-to-obstacle distances. Moreover, [6], [8] use 3D laser sensors, which are naturally able to obtain the robot-to-obstacle distance.

In regards to network architectures proposed for laser data processing, Pfeiffer *et al.* [10] trained a Deep Neural Network (DNN) end-to-end to mimic a motion planner with laser data as input and velocity commands as output. The training data was obtained from simulation but validated on a real robot navigating complex corridors. In that work the authors propose a neural network architecture specifically tailored to process laser data: it consisted of a fully Convolutional Neural Network (CNN), using Batch Normalizations (BNs), Rectified Linear Units (ReLUs) and skip connections (details about these structures is given in Sect. III). Despite good results which validated the network structure, the authors claimed the learned motion planner underperformed when in wide open areas with a lot of glass and/or clutter, a problem that is partly due to missing obstacles in laser data and that we address in this work.

The problem of undetected obstacles when using 2D laser scans was also mentioned in the work by Liao *et al.* [9], where they used 2D laser scans together with RGB images to predict a 3D depth map of the same scene by a Residual Neural Network (ResNet). Although the method was not per se developed for obstacle detection and avoidance, it was experimentally shown to successfully detect obstacles that were not seen from the fixed 2D laser. However, to produce such measurements the algorithm still relies on integrating information from RGB images.

Along the same line of inferring missing obstacles in laser data with vision, Baltzakis *et al.* [1] proposed a method which at runtime fuses laser and visual data, and is an example of sensor fusion. The method constructs a local 3D model from laser scans which, in turn, is visually evaluated by a stereo vision system to detect incorrect models. In such cases, the model is corrected with the depth data from the visual sensor. The method was successfully tested in simulation and on a real robot navigating a corridor filled with tables, chairs, and open doors. Although the problems

addressed in sensor fusion works such as [1], [9] are in essence the same as in this work, those methods require overlapping readings from camera and laser sensors, which our method does not.

## III. METHOD

Let us define the output of a generic  $N$ -point 2D laser positioned at a height  $h$  from floor level as a 1D vector  $\mathbf{l}_h = \{l_{ih}\}_{i=1}^N$  where each  $l_{ih}$  represents an estimate (usually, in meters) of the distance  $d_{ih}$  of closest obstacle from the laser along the direction  $i$  at height  $h$ . When considering a specific robot model having a 2D laser sensor positioned at a fixed height  $h^* \in [0, H]$ , where 0 is floor level and  $H$  is the robot height, we define the vector  $\mathbf{x} = \{x_i \mid x_i = l_{ih^*}\}_{i=1}^N$ .

In this work we address the problem of predicting robot-to-obstacle distances, given an  $N$ -point 2D range laser acquisition  $\mathbf{x}$ . The robot-to-obstacle distances are represented as  $\mathbf{y} = \{y_i\}_{i=1}^N$ , *i.e.*, in the same space as the input laser  $\mathbf{x}$ . Formally, we can define each  $y_i$  as

$$y_i = \min_{h \in [0, H]} d_{ih} . \quad (1)$$

In particular, we want to learn the function  $\mathcal{H} : \mathbb{R}^N \rightarrow \mathbb{R}^N$  for which  $\mathcal{H}(\mathbf{x}) = \mathbf{y}$ . To this end, following the intuition behind the work by Pfeiffer *et al.* [10], we propose to train a fully convolutional autoencoder architecture. An autoencoder is a deep learning architecture that can be formalized as a pair of transformations  $\phi$  and  $\psi$  such that:

$$\begin{aligned} \phi : \mathbb{R}^N &\rightarrow \mathbb{R}^m , \\ \psi : \mathbb{R}^m &\rightarrow \mathbb{R}^N . \end{aligned} \quad (2)$$

Traditionally autoencoders were proposed in unsupervised settings [11], [12] to reconstruct the input, *i.e.*, to compute the *latent variable*  $\mathbf{z} = \phi(\mathbf{x}) \in \mathbb{R}^m$  and then reconstructing the original input as  $\mathbf{x} = \psi(\mathbf{z})$ , given a loss function  $\mathcal{L}$ ,

$$\phi, \psi = \arg \min_{\phi, \psi} \mathcal{L}((\psi \circ \phi)\mathbf{x}, \mathbf{x}) . \quad (3)$$

In that setting typically  $m < N$ , and the signal  $\mathbf{x}$  is effectively compressed in the representation  $\mathbf{z}$ . For this reason,  $\phi$  and  $\psi$  are typically referred to as *encoder* and *decoder* respectively.

In contrast, we propose to use an autoencoder to predict  $\mathbf{y}$  instead of reconstructing  $\mathbf{x}$ . This moves us from an unsupervised to a supervised learning setup, and for this reason knowledge of the correct  $\mathbf{y}$ , *i.e.*, a ground truth, is required to train the network. We will discuss in detail how we propose to empirically obtain  $\mathbf{y}$  in Sect. IV-B.

### A. Network architecture

A graphical representation of the proposed network structure is given in Fig. 2. The encoder  $\phi$  takes as input a 1D vector  $\mathbf{x}$  of size  $N = 128$  and passes it through four 1D convolutional layers, with kernel size 5 and stride 2, connected via BN [13] and ReLU [14] layers. The input vector  $\mathbf{x}$  is scaled to the range  $[0, 1]$  before feeding it to the network. The output of the encoder is reshaped to obtain the latent feature representation  $\mathbf{z}$ . The decoder  $\psi$  has the

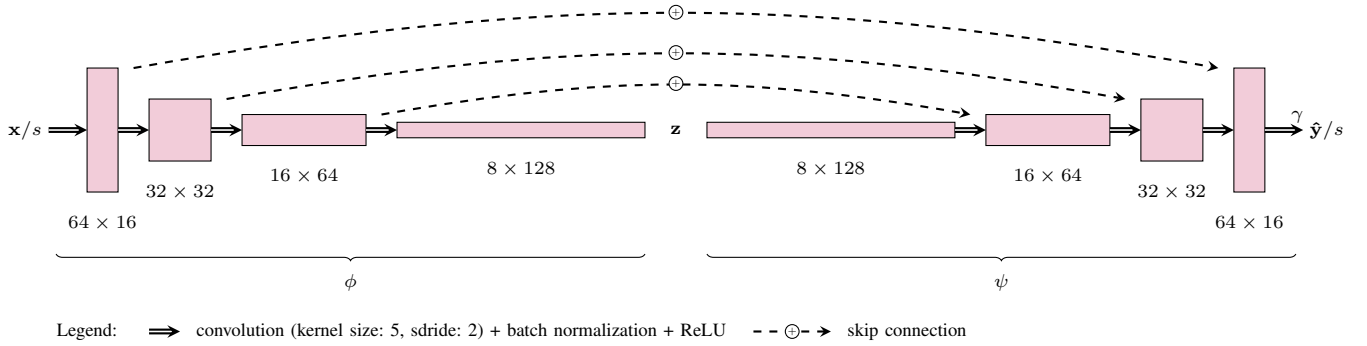


Fig. 2. The proposed fully convolutional autoencoder

same structure as  $\phi$ , which maps  $\mathbf{z}$  back to a 1D vector  $\hat{\mathbf{y}}$  of size  $N$  through a series of 1D transposed convolutional (often, improperly, referred to as deconvolutional) layers of kernel size 5 and stride 2 connected via BN and ReLU. In the next sections we will discuss some components of the network architecture and the intuitions rooted in the specific laser data domain that justifies them. The actual contribution of these components to the performance of the network is evaluated in Sect. IV.

### B. Skip connections

We propose to connect corresponding convolutional and deconvolutional layers through skip connections, as shown in Fig. 2. Previous works [10], [15], [16] demonstrated a two-folded contribution of such connections: firstly they improve gradient back-propagation to bottom layers and secondly they increase the flow of detail information to top layers.

The way skip connections work is that the output of a convolutional layer in the encoder is added to the output of the corresponding deconvolutional layer of the same size in the decoder. The result is then used as the input of the next deconvolutional layer. This operation allows high frequencies that are typically lost by the encoder to be passed to the decoder to produce a more detailed reconstruction.

### C. Non-uniform scaling

Both the input laser  $\mathbf{x}$  and the output obstacle vector  $\mathbf{y}$  represent distance measures in meters with values in range  $[0, s]$  where  $s$  is the maximum laser distance (in our work, 30 m). Intuitively, for the robot to safely navigate, an error in the distance estimate for a closer object is far more dangerous than for an object far away; for this reason accurate prediction in the first couple of meters is crucial. However, when considering the range of a typical laser, the first couple of meters are residing in a small fraction of the range. To address this issue, we propose to first scale the input in the range  $[0, 1]$  by linear scaling, and then scale the output of the last layer of the network  $\hat{\mathbf{y}}'$  by a positive  $\gamma$  factor, before bringing it back to its original range. Formally,

$$\mathbf{x}' = \mathbf{x}/s, \quad (4)$$

$$\hat{\mathbf{y}}' = (\psi \circ \phi)\mathbf{x}', \quad (5)$$

$$\hat{\mathbf{y}} = s(\hat{\mathbf{y}}')^\gamma. \quad (6)$$

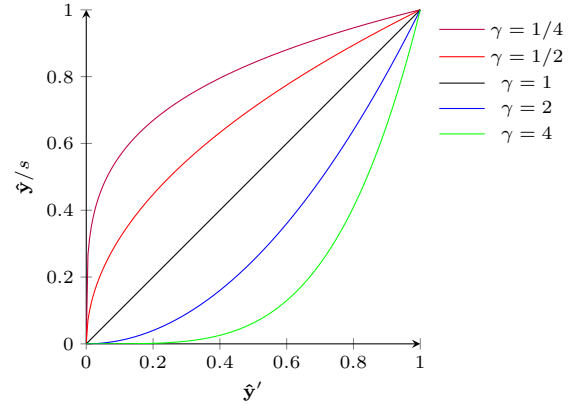


Fig. 3. Effect of different values of  $\gamma$  on the output of the last layer of the network.

The intuition behind this non-uniform output scaling, which henceforth is referred to as  $\gamma$ -scaling, comes from the domain of image processing, where *gamma correction* is used to enhance contrast in an image and *gamma encoding* is used to optimize the bandwidth used to transport an image according to the way humans perceive light and color.

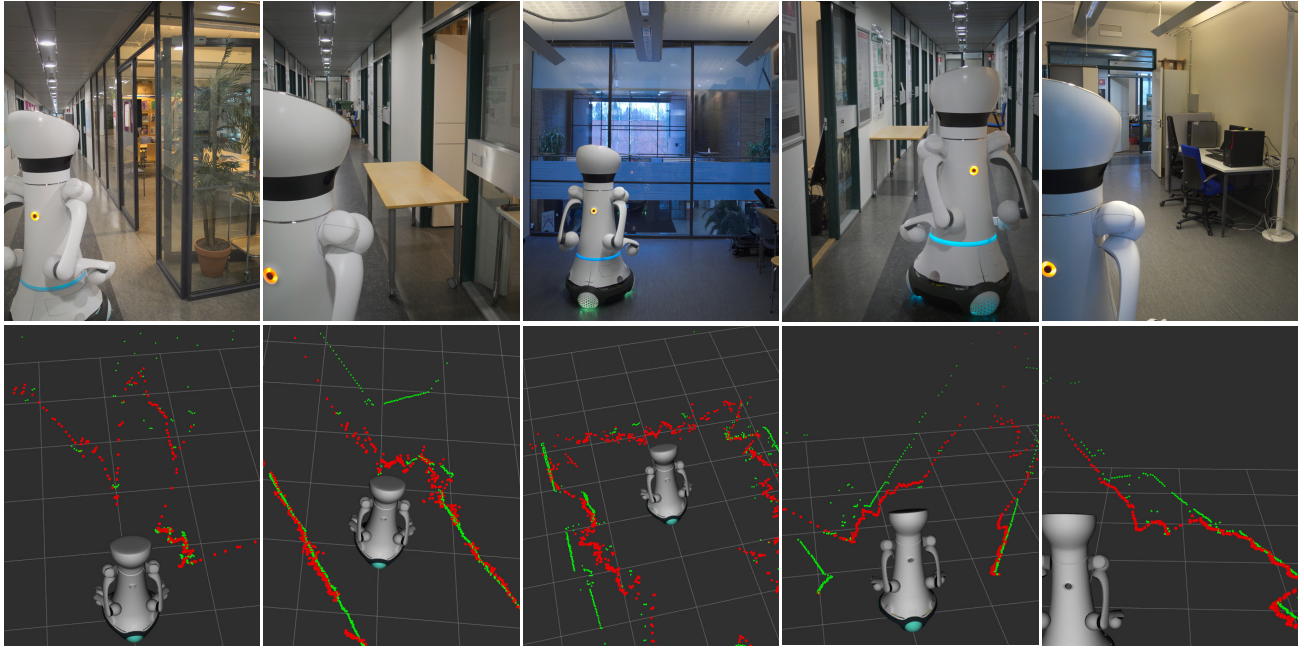
The effect of different values of  $\gamma$  is shown in Fig. 3. By using  $\gamma > 1$ , a greater portion of the range of the last layer of the network is reserved for the smallest values of the output, effectively increasing the resolution in that portion of the range while reducing the resolution for the rest of the output range. Using  $0 < \gamma < 1$  yields the opposite effect instead, which in our case is not desired.

### D. Loss function

Following the same reasoning as in Sect. III-C, we trained the network using Root Mean Squared Logarithmic Error (RMSLE) as loss function. RMSLE can be expressed as:

$$\begin{aligned} \mathcal{L}(\hat{\mathbf{y}}, \mathbf{y}) &= \sqrt{\frac{1}{N} \sum_{i=1}^N [\ln(\hat{y}_i + 1) - \ln(y_i + 1)]^2} \\ &= \sqrt{\frac{1}{N} \sum_{i=1}^N \ln^2 \frac{\hat{y}_i + 1}{y_i + 1}}; \end{aligned} \quad (7)$$

it is a common choice for domains in which the desire is to mitigate the contribution of big errors when numbers are big themselves.



(a) Room with glass walls (b) Table blocking a door (c) Glass window (d) Table in a corridor (e) Table and chairs

Fig. 4. Examples of scenes encountered while testing on the Care-O-bot 4; the green laser is the original input signal, while the red one is the output produced in real-time by the proposed algorithm (best viewed in color).

It is important to note that by using  $\gamma > 1$ , the network imposes variable output resolution to produce smaller errors for smaller numbers while admitting larger errors for bigger numbers. It is therefore important to pair this choice with a loss function that follows the same idea. If Mean Squared Error (MSE) was used, the error for big numbers could possibly overshadow more important smaller errors and negatively impact the learning process.

#### IV. EXPERIMENTS AND RESULTS

##### A. Experimental Platform

In this work we used the mobile service robot Care-O-bot 4 shown in Fig. 1 and Fig. 4. The robot is equipped with omni-directional wheels and three 2D SICK S300 safety laser scanners, one at front, one to the left, and one to the right, with maximum scanning range of 30 m, resolution of 30 mm and angular resolution of  $0.5^\circ$ . Together all three lasers scanners enable the robot to sense its  $360^\circ$  surrounding. Furthermore, the robot is equipped with three RGBD Asus Xtion cameras located at the front of the robot together covering a field of view of approximately  $90^\circ$ . As a consequence, the robot senses only about  $90^\circ$  of its surrounding with overlapping laser and image sensors while the remaining  $270^\circ$  are sensed using laser scanners alone. This sensing limitation motivated the work in this paper as our method enables inferring robot-to-obstacle distances from laser data without requiring additional sensors.

##### B. Dataset

As already mentioned in Sect. III, we are training in a supervised learning setting, which requires matching pairs

of input laser data  $\mathbf{x}$  and robot-to-obstacle distance vectors  $\mathbf{y}$ . We therefore acquired a dataset composed of laser scans, serving as input, and corresponding depth images of the same scene obtained from one of the front-facing cameras on the Care-O-bot 4. Then, the depth images were projected to 1D by iteratively taking the closest distance of each column in the depth image and storing it as the distance vector estimated by the depth camera. Furthermore, to focus on obstacles that the robot could collide with, we removed from the depth images all points that, once converted to the 3D space, were outside the range  $[\epsilon, H]$  with  $\epsilon = 0.05$  m. Additionally, as the field of view of a single laser scanner is about  $270^\circ$  while only  $90^\circ$  are covered by the RGBD sensors, it was necessary to prune the laser scan until it matches the field of view of the camera. Once the matching was complete we obtained two 1D vectors of size  $N = 128$ , one originated from the laser scanner and one obtained from the depth camera, which we will refer as  $\mathbf{x}$  and  $\mathbf{y}^c$  respectively. Then we set  $\mathbf{y}$  as

$$\mathbf{y} = \{y_i = \min(x_i, y_i^c)\}_{i=1}^N . \quad (8)$$

The final step forces the ground truth to consist of the closest points from either sensor readings to provide a conservative estimate of the obstacle distance. An example of  $\mathbf{x}$ ,  $\mathbf{y}^c$ , and  $\mathbf{y}$  is shown in Fig. 5.

This approach of generating the ground truth from depth images provided us with a good estimate of the robot-to-obstacle distance, did not require manual labeling, and enabled us to acquire a dataset directly by running the robot around. However, generating similar ground truth would be also possible from, for example, an accurate map of the

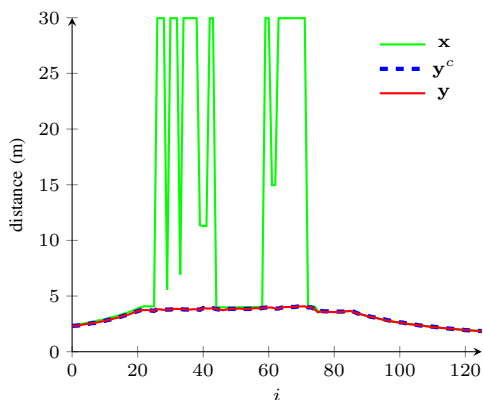


Fig. 5. Sample data from the training dataset. This reading is taken while the robot is facing a closed two-panel glass door.

environment, or human labeling.

We gathered the dataset by teleoperating the Care-O-bot 4 in a university building. We gathered a training set consisting of 27904 input-output pairs in the second floor of the building, while the test set was obtained in the third floor and consists of 11604 input-output pairs. Several of these locations included glass surfaces, tables and chairs, *e.g.*, those shown in Fig. 4, whose robot-to-obstacle distance is incorrectly inferred by the laser scanner but correctly estimated by the depth image, capturing interesting evaluating scenarios for the network to represent. Although the two floors present structural similarities, we argue they vary enough in the overall topology and obstacle content to act as a good train-test set pair. Nevertheless, in future works we aim at expanding both the training and test set with data from various indoor environments.

### C. Data augmentation

In other domains [17]–[19] it is known that injection of noise in the input of the training dataset can improve the generalization capability of neural networks and encourages a network to converge to smoother mapping functions. However, to the best of our knowledge, this has never been tested when training on laser. Therefore, during training, we augmented the data by adding random noise sampled from a Gaussian distribution  $\mathcal{N}(0, \sigma_n)$  to the input. In this study, we set  $\sigma_n = 0.02\text{m}$ , which is compatible with the sensor resolution of the Care-O-bot 4. In the next section we evaluate and discuss the contribution of noise injection on training performance.

In addition, to further increase variability in the training set, for each training example, a random 50% chance of flipping both  $x$  and  $y$  has been implemented. This way, the number of samples in the training dataset effectively doubles.

### D. Evaluation on test set

All networks evaluated in this work were implemented in pyTorch 0.3.0 and trained for 2000 epochs on the augmented training dataset presented in the previous sections by using shuffled batches of 32 samples. The networks were trained

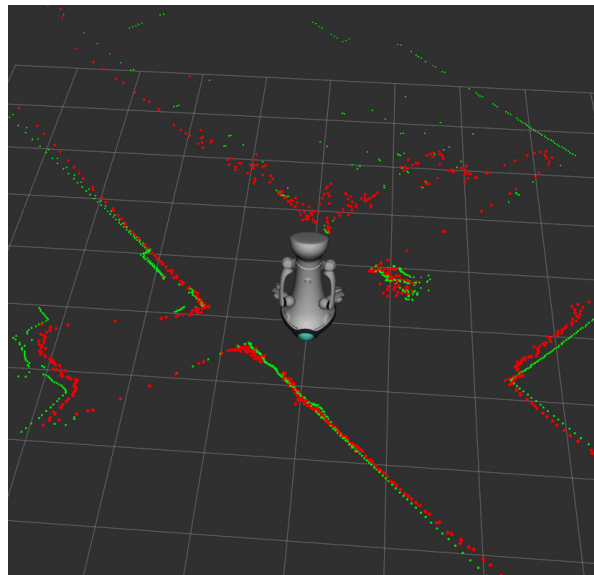


Fig. 6. 360° laser hallucination; the green laser is the original input signal, while the red one is the output produced in real-time by the proposed algorithm (best viewed in color).

using RMSLE as loss function and optimizing with Adaptive Moment Estimation (Adam) [20].

We are in particular interested in evaluating whether skip connections,  $\gamma$ -scaling and the injection of noise increase the performance. To quantitatively evaluate their contributions and the effective ability of the proposed architecture to learn the true obstacle distances from laser data, we trained each network configuration 5 times. The results, in terms of mean and standard deviation of the RMSLE, are presented in Tab. I. The configuration n. 0 is taken as baseline, *i.e.*, the one including all hyperparameters presented in this work. Configurations n. 1-5 are obtained by changing only one of the hyperparameters at the time, while configuration n. 6 is obtained by having all proposed hyperparameters disabled. This approach enabled us to evaluate the contribution of each single component to the performance.

From the results presented in Tab. I, it is clearly seen that among all hyperparameters, the inclusion of skip connections improves the network performance the most. Additionally, it can be concluded that using a value of  $\gamma > 1$  is a good choice for this domain. However, as is predictable, a too high value, as in the case of  $\gamma = 4$ , limits improvements due to exaggerated scaling. Finally, it is interesting to notice the effect of the inclusion of noise: the negligible deficit to the average performance it produces is counterbalanced by an almost halved standard deviation; which seems to confirm the results presented in [17]–[19], where the main contribution of injecting noise into the training inputs was claimed to be an increased ability of the network to learn more consistent results. Configuration n. 6, *i.e.*, the one having all hyperparameters excluded, performs the worst, confirming once more the positive effect all proposed hyperparameters have on performance.

TABLE I  
TEST-SET PERFORMANCE AND PARAMETER CONTRIBUTIONS

n.	Network hyperparameters			RMSLE (absolute)		RMSLE (relative to n. 0)	
	Skip connections	$\gamma$	$\sigma_n$	mean ( $\times 10^{-2}$ )	std ( $\times 10^{-3}$ )	mean	std
0	✓	2	0.02	2.865	0.31		
1		2	0.02	3.059	1.45	+6.79%	+372.81%
2	✓	2		2.838	0.57	-0.95%	+84.82%
3	✓	½	0.02	2.885	1.27	+0.71%	+315.13%
4	✓	1	0.02	2.938	1.01	+2.54%	+230.12%
5	✓	4	0.02	2.869	0.47	+0.13%	+52.35%
6		1		3.065	0.76	+6.98%	+148.91%

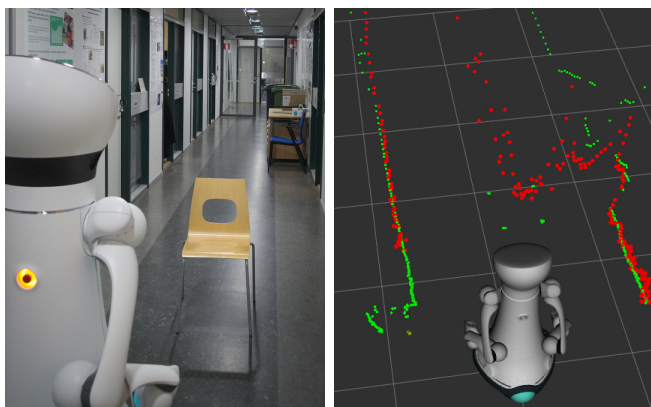


Fig. 7. A problematic sample; the green laser is the original input signal, while the red one is the output produced in real-time by the proposed algorithm (best viewed in color).

#### E. Online testing on the Care-O-bot 4

Based on the quantitative results in Tab. I, the network with skip connections,  $\gamma = 2$ , and trained with zero mean Gaussian noise with standard deviation  $\sigma_n = 0.02$  provided the best results. The same network was further tested online on Care-O-bot 4 in the same office spaces from which the training and test sets were gathered. The reason for testing on the same floor as the training set was because this floor included many challenging situations such as the room with glass walls and doors presented in Fig. 4a. Additionally we changed the environment by, for example, relocating tables to close access to corridors (Fig. 1) and doors (Fig. 4b), creating situations not present in the training set. Other test scenarios included a glass window covering an entire wall (Fig. 4c) and a table with chairs underneath (Fig. 4e).

The figures show that the trained network is able to hallucinate laser data that better estimates the robot-to-obstacle distance. Particularly impressive results occur when the robot faces the room with glass walls in Fig. 4a and correctly recognizes the door from other walls. It is also worth pointing out that the network can infer missing laser data from a small set of points corresponding to obstacles such as the table in Fig. 4d. Although the network was trained on data gathered from a  $90^\circ$  viewing angle, it is possible to hallucinate  $360^\circ$  around the robot as shown in Fig. 6 by running the network on laser chunks of that size.

In most testing situations the proposed approach produced

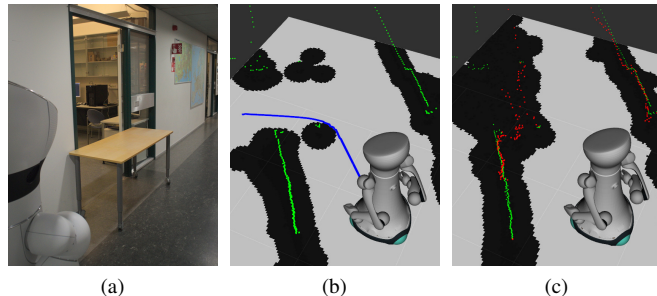


Fig. 8. Comparison of the behaviour of a local planner relying on raw laser data (b) or on hallucinated laser data (c) while the robot is instructed to plan a trajectory through a door obstructed by a table; in both pictures the white area is considered free space, the black areas are considered obstructed, the blue line is the planner trajectory, the green laser is the original input signal, while the red one is the output produced in real-time by the proposed algorithm (best viewed in color).

correct results, even when we changed object locations to ones the network never saw during training. Nevertheless, we noticed that the trained network was unable to correctly infer robot-to-obstacle distance in scenarios greatly different from the training set. For example, tables were correctly detected even if moved to new locations as long as they were parallel to a wall, but if placed perpendicular they were not correctly detected. Similarly, as shown in Fig. 7, objects positioned alone in the middle of empty spaces were not correctly detected. Both these situations were not present in the training set and were therefore not learned by the network. To address this issue we want to explore more thorough data augmentation in the future, for example by synthetically injecting objects in random positions in the data. Another interesting network behavior is the tendency to produce smooth curves even in presence of strong discontinuities. This phenomenon is visible for the doors shown in Fig. 6, the corridor however was correctly kept open. Although such behavior is not problematic most of the times, it can cause navigation issues when planning through a door, as some navigation goals may seem unreachable. The smoothing tendency stems from the network topology, and to overcome it one solution is to more aggressively enforce non-linearities in the network structure.

Finally, we tested the use of the hallucinated laser for autonomous local navigation. Fig. 8 shows an example where the robot was given a navigation goal inside the room. The

planner using only raw laser planned a trajectory through the table (the blue line in Fig. 8b) which would cause a collision, while the one relying on the hallucinated laser did not as it successfully inferred the actual robot-to-obstacle distance as shown in Fig. 8c.

## V. CONCLUSIONS AND FUTURE WORK

Detecting and inferring distance to complex obstacles from 2D laser scans alone is nontrivial but useful for robot safety. In this work, we presented a method capable of estimating the robot-to-obstacle distance from raw 2D laser data. This is achieved by framing the problem as a learning task and training a DNN to infer the robot-to-obstacle distances from the laser scans. The key concept is to shape the DNN as an autoencoder with skip connections between each convolutional and deconvolutional layer, enabling the network to pass detailed information from bottom to top layers. Furthermore, to generate the actual training and test set we proposed a method to estimate the true distance to obstacles by fusing 2D laser data and depth images. Based on the quantitative evaluation on the test set, the network with skip connections outperformed the ones without, and by further adding noise to the input data and shaping the last layer using a novel non-uniform  $\gamma$ -scaling the overall performance increased while the standard deviation decreased, resulting in more robust learning. The real robot test demonstrated that the trained network was able to infer the robot-to-obstacle distance in 360° in challenging situations including an entire wall made of glass windows or from a scarce set of laser points that corresponded to the obstacle as in the case of tables.

To the best of our knowledge no prior work has focused on problems similar to the one presented here, opening up interesting future research avenues. To improve generalization, the training dataset could be augmented by domain randomization, corresponding to changing location and rotation of objects such as tables, chairs, or windows. To enable prediction of moving obstacles, for example walking humans, a temporal component could be included in the network along the lines of [7]. Finally, the ideas presented in this work could be integrated with end-to-end training for navigation, by extending a motion planner similar to the one in [10].

## REFERENCES

- [1] H. Baltzakis, A. Argyros, and P. Trahanias, "Fusion of laser and visual data for robot motion planning and collision avoidance," *Machine Vision and Applications*, vol. 15, no. 2, pp. 92–100, Dec. 2003.
- [2] F. Bonin-Font, A. Ortiz, and G. Oliver, "Visual Navigation for Mobile Robots: A Survey," *Journal of Intelligent and Robotic Systems*, vol. 53, p. 263, Nov. 2008.
- [3] H. Surmann, A. Nüchter, and J. Hertzberg, "An autonomous mobile robot with a 3d laser range finder for 3d exploration and digitalization of indoor environments," *Robotics and Autonomous Systems*, vol. 45, no. 3, pp. 181–198, Dec. 2003.
- [4] W. Burgard, A. B. Cremers, D. Fox, D. Haehnel, G. Lakemeyer, D. Schulz, W. Steiner, and S. Thrun, "Interactive museum tour-guide robot," in *Proceedings of the National Conference on Artificial Intelligence*. AAAI, 1998.
- [5] J. Sergeant, N. Sünderhauf, M. Milford, and B. Upcroft, "Multimodal Deep Autoencoders for Control of a Mobile Robot," in *Proceedings of the Australasian Conference on Robotics and Automation 2015 (ACRA 2015)*. Canberra, Australia: ARAA, 2015, pp. 1–10.
- [6] B. Li, T. Zhang, and T. Xia, "Vehicle Detection from 3d Lidar Using Fully Convolutional Network," in *Robotics: Science and Systems XII*, vol. 12, June 2016.
- [7] P. Ondruska and I. Posner, "Deep Tracking: Seeing Beyond Seeing Using Recurrent Neural Networks," in *Thirtieth AAAI Conference on Artificial Intelligence*, Mar. 2016.
- [8] M. Engelcke, D. Rao, D. Z. Wang, C. H. Tong, and I. Posner, "Vote3deep: Fast object detection in 3d point clouds using efficient convolutional neural networks," in *2017 IEEE International Conference on Robotics and Automation (ICRA)*, May 2017, pp. 1355–1361.
- [9] Y. Liao, L. Huang, Y. Wang, S. Kodagoda, Y. Yu, and Y. Liu, "Parse geometry from a line: Monocular depth estimation with partial laser observation," in *2017 IEEE International Conference on Robotics and Automation (ICRA)*, May 2017.
- [10] M. Pfeiffer, M. Schaeuble, J. Nieto, R. Siegwart, and C. Cadena, "From perception to decision: A data-driven approach to end-to-end motion planning for autonomous ground robots," in *2017 IEEE International Conference on Robotics and Automation (ICRA)*, May 2017, pp. 1527–1533.
- [11] Y. Bengio, *Learning Deep Architectures for AI*. Now Foundations and Trends, 2009.
- [12] D. D. Testa and M. Rossi, "Lightweight Lossy Compression of Biometric Patterns via Denoising Autoencoders," *IEEE Signal Processing Letters*, vol. 22, no. 12, pp. 2304–2308, Dec. 2015.
- [13] S. Ioffe and C. Szegedy, "Batch Normalization: Accelerating Deep Network Training by Reducing Internal Covariate Shift," in *PMLR*, June 2015, pp. 448–456.
- [14] K. He, X. Zhang, S. Ren, and J. Sun, "Delving Deep into Rectifiers: Surpassing Human-Level Performance on ImageNet Classification," in *2015 IEEE International Conference on Computer Vision (ICCV)*, Dec. 2015, pp. 1026–1034.
- [15] X. Mao, C. Shen, and Y.-B. Yang, "Image Restoration Using Very Deep Convolutional Encoder-Decoder Networks with Symmetric Skip Connections," in *Advances in Neural Information Processing Systems 29*, D. D. Lee, M. Sugiyama, U. V. Luxburg, I. Guyon, and R. Garnett, Eds. Curran Associates, Inc., 2016, pp. 2802–2810.
- [16] A. Newell, K. Yang, and J. Deng, "Stacked Hourglass Networks for Human Pose Estimation," in *Computer Vision – ECCV 2016*, ser. Lecture Notes in Computer Science. Springer, Cham, Oct. 2016, pp. 483–499.
- [17] L. Holmstrom and P. Koistinen, "Using additive noise in back-propagation training," *IEEE Transactions on Neural Networks*, vol. 3, no. 1, pp. 24–38, Jan. 1992.
- [18] K. Matsuoka, "Noise injection into inputs in back-propagation learning," *IEEE Transactions on Systems, Man, and Cybernetics*, vol. 22, no. 3, pp. 436–440, May 1992.
- [19] S. Yin, C. Liu, Z. Zhang, Y. Lin, D. Wang, J. Tejedor, T. F. Zheng, and Y. Li, "Noisy training for deep neural networks in speech recognition," *EURASIP Journal on Audio, Speech, and Music Processing*, vol. 2015, no. 1, p. 2, Dec. 2015.
- [20] D. P. Kingma and J. Ba, "Adam: A Method for Stochastic Optimization," *arXiv:1412.6980 [cs]*, Dec. 2014, arXiv: 1412.6980.